Aerosol Direct Radiative Forcing with an AERONET touch

S.Kinne, MPI-Meteorology, Hamburg
AeroCom global modeling community
AERONET sun-/sky- photometry

1. Introduction

Aerosol introduces one of the largest uncertainties in climate research. Aerosol originates from different sources and has short lifetimes on the order of a few days. Thus, aerosol properties (characterized by amount, size and composition) and their vertical distribution vary strongly by location and in time. Complicating factors to assessments of the aerosol impact on climate are uncertainty and the variability of environmental properties such as clouds and surface properties, which modulate the aerosol associated impact. The impact of any atmospheric change is commonly quantified by radiative forcing, the imposed change to the radiative energy balance. In particular, changes at the top of the atmosphere (ToA) are of interest, because they summarize the overall impact on the Earth's climate. For aerosol, the ToA radiative forcing changes in magnitude and even in sign, depending on local aerosol and environmental properties and the overall (spectrally, daily and regionally integrated) impact (often a difference larger numbers) is highly uncertain – even when integrating over time.

Here results from radiative transfer simulations are presented. These calculations only address the impact due to the presence of aerosol in the atmosphere (direct effect). The calculations do not include aerosol interactions with clouds and/or the hydrological cycle (indirect effects). These time-dependent feedback processes can only be adequately explored in more complex (global) circulation models. For estimates of the aerosol direct effects, the necessary input on aerosol properties and associated environmental properties in this study is based on monthly statistics from remote sensing samples which were globally and spatially extended by model ensemble median fields to yield complete data-sets.

First the aerosol data-sets and the environmental data-sets are introduced, then the calculations are explained, forcing results are presented and eventually comparisons to published estimates are presented.

2. Data

Aerosol impacts on the solar (SOL) and terrestrial-infrared (IR) energy balance are quantified in (broadband) radiative transfer simulations, which require spectrally resolved data on aerosol optical properties and environmental conditions. These data must have sufficient temporal resolution to resolve seasonal aspects. And these data must have global coverage to address the global aspect of climate. In this study data-sets are applied, which summarize monthly statistics at a coarse (1^{o}longitude and 1^{o}latitude) horizontal resolution. Available data of environmental data-sets (e.g. clouds, solar surface albedo) were combined with newly developed data-sets for aerosol, which can be considered as initial efforts to develop a new climatology for aerosol. First, the creation of these new aerosol data-sets explained. Here, an effort was made to involve as many quality aerosol measurements as possible. Nonetheless, modeling support was needed to complete and extend measurements in terms of (spatial and temporal) coverage and detail. Next, the applied environmental data-sets are introduced. And finally, simulated aerosol radiative forcing fields are presented and discussed in the context of other available estimates.

Aerosol properties

Aerosol is usually defined by amount, size, composition and shape. The equivalent optical properties are aerosol optical thickness (‘aot’), single scattering albedo (‘ssa’) and phase-function (‘P’) or asymmetry-factor (‘g’). The ‘aot’, the vertically integrated extinction, is a measure for (direct) attenuation, due to all scattering and all absorption events. Further details on these interactions are provided by the other two properties. The ‘ssa’ indicates the likelihood of a scattering event as opposed to an absorption event (ssa=0: absorption only, ssa=1: scattering only). In other words, the co-single scattering albedo ‘1-ssa’ is a direct measure for the absorption potential of aerosol. ‘P’ defines the re-distribution of radiation after a scattering event. The details of ‘P’ are commonly approximated by a function, which can be represented by a single value, ‘g’ (g= +1: all forward directed, g= -1: all backward directed). Since forward scattering strength is correlated with particles size, the value of ‘g’ is also a general indicator for size. Usually, the shape of a sphere is assumed, since the approximation of ‘P’ by ‘g’ breaks down for non-spheres. For any aerosol (-distribution), all three properties (‘aot’, ‘ssa’ and ‘g’) vary with wavelength, due to changes in the size-wavelength ratio and due to spectral absorption features of the aerosol composition. Since radiative forcing simulations are usually expected to summarize the impact from interactions at all solar and (terrestrial) infrared wavelengths, the spectral dependency of all three aerosol properties must be included. Clearly, the most important spectral sub-region for (sub-micron size) aerosol is the mid-visible (due size-wavelength ratio related cross-sections and the maximum in available solar radiation). At 0.55μm, a common mid-visible reference wavelength in modeling, typical values for tropospheric aerosol are 0.15 (‘aot’), 0.93 (‘ssa’) and 0.7 (‘g’).

The primary effort will be the preparation of global (1^{0}longitude*1^{0}latitude) monthly statistics for the vertical column properties of ‘aot’, ‘ssa’ and ‘An’ at 0.55μm, where ‘g’ has been replaced by the easier to measure Angstrom parameter (‘An’). The Angstrom parameter represents the (mid-visible) ‘aot’ spectral dependence via the negative slope in log-space and provides a direct link to ‘g’ over the size-connection (sub-micron particles: ‘An’ >1.2 and g ~0.65; super-micron particles: ‘An’ <0.5, g ~0.75). For the development of global aerosol

data-sets, three data sources are considered: Remote sensing from space, remote sensing from ground networks and results from model simulations.

1. ***Remote sensing from space*** can retrieve a subset of aerosol properties (usually 'aot' and its spectral dependence for 'An' estimates) with a-priori assumptions to other aerosol properties (at least aerosol absorption) and environmental properties. Without sufficient accuracy to these assumptions, satellite aerosol retrievals fail, in particular over land and brighter surfaces (e.g. desert, sun-glint over ocean). In addition, global coverage is usually accomplished with polar-orbiting satellite which provide at best one day-time overpass. Considering that a successful aerosol retrieval requires a cloud-free scene, the temporal sampling often becomes so sparse, that even monthly averages at 1*1 (^{0}lon, ^{0}lat) horizontal resolution lack statistical significance. Thus, data from multi-year data-sets are combined (excluding periods of enhanced stratospheric loading) to provide global data-sets, more so on general distribution rather than absolute accuracy, as exemplified for 'aot' in Figure 1.

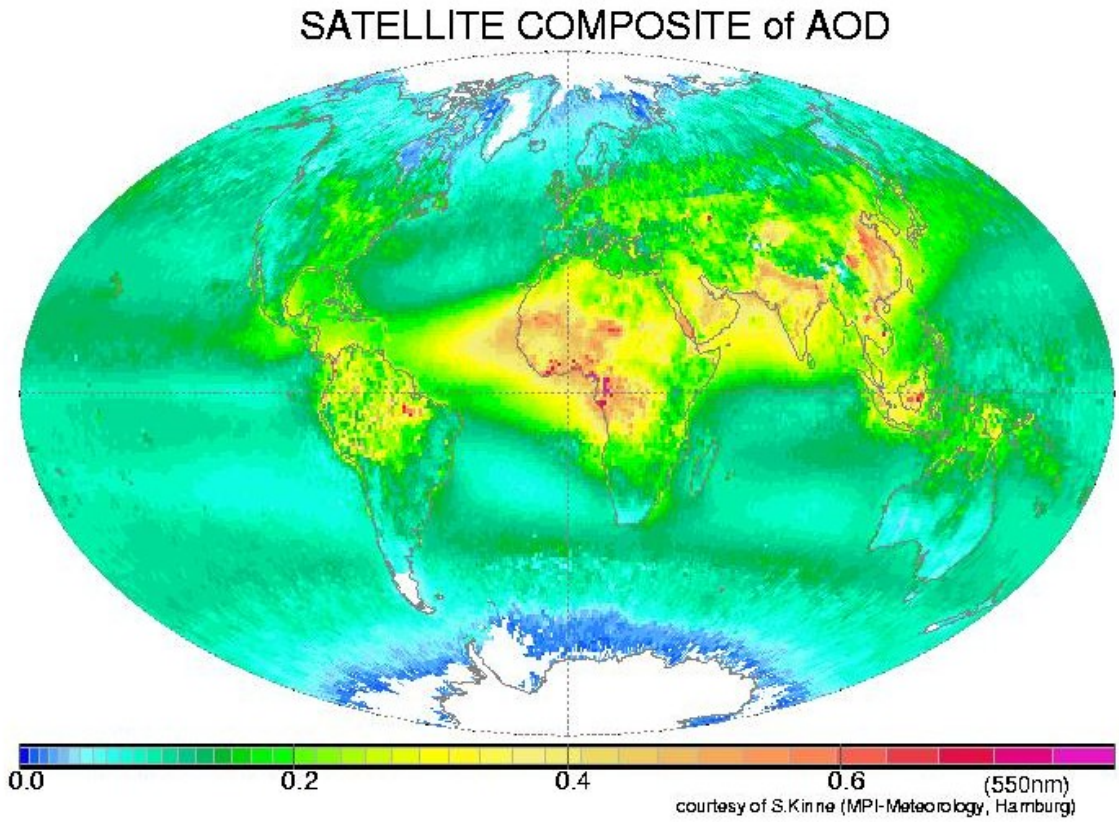

Figure 1. Annual aerosol optical depth composite of different multi-annual aerosol retrievals based on a agreement to more accurate ground remote sensing on a regional basis

The accuracy of satellite retrievals will improve as simultaneous data of more detail and higher accuracy from ground remote sensing or in-situ samples provide stronger constraints to satellite improve retrieval assumptions.

2. ***Remote sensing from ground*** can provide data on all three aerosol properties ('aot', 'ssa' and 'An'). In particular, measurements of direct solar attenuation permit highly accurate data for 'aot' and 'An'. Additional measurements near the sun allow reliable estimates for the aerosol size-distribution, and additional sky-radiance measurements provide estimates on aerosol absorption (and 'ssa') at sufficient aerosol loading. This makes surface-instrumentation with sky-sun photometry sensors particular appealing – especially if many surface sites are connected through cross-calibrations to networks, such as for AERONET (Holben et al. 1998). A higher (compared to satellite retrievals) temporal resolution allows for much better statistics, although the requirement for cloud-free scenes remains. Major handicaps in terms of global data are the potential for local biases, such that site statistics may not qualify as regional (1^0*1^0) average and the uneven (land) site distribution.

3. ***Modeling*** alone can provide (spatially and temporally) complete and consistent data-sets for all aerosol properties. However, there are questions regarding many underlying assumptions (e.g. emissions, water-affinity) and parameterizations (e.g. cloud-aerosol interactions). Model validations are largely confined to integrated properties, which are insufficient to assess sub-processes. This lead to an international effort called AeroCom (Kinne et. al., 2005) which seeks to diagnose aerosol modules in global modeling. To capture the essence of current skill in aerosol global modeling, aerosol fields of the model median were created: Once all 16 AeroCom models were re-gridded to the same 1*1 (^{0}lon, ^{0}lat) horizontal resolution, always the center value was picked at each model grid separately for each month (eliminating outliers, which otherwise would have affected the average).

The new (mid-visible) aerosol climatology

The AeroCom monthly median fields for the three aerosol properties of 'aot', 'ssa' and 'An' (as illustrated in the Appendix of Kinne et al. 2005) provide the starting point to a more measurement based (new) aerosol climatology. The overall idea is overwrite the model median fields in regions where quality statistics from remote sensing can be provided (for any particular month). In terms of applied remote sensing input, ground data from AERONET sites are preferred over satellite data-sets, due to advantages in terms of accuracy and number of retrieved properties. The AERONET quality assured data pool by 2005 covered 304 sites with at least one month of more than 50 attenuation samples (sun-data: 'aot', 'An') and 239 sites with at least one month of 10 inversion samples (sky-data: 'ssa'). The merging of AERONET statistics with model median fields occurs in five steps:

1. rate local AERONET sites in terms of quality and regional characterization

Each AERONET site is assigned a quality score (3, 2, 1or 0) and a range score (3, 2, 1, 0) based on site assessments by the AERONET staff (T. Eck, personal communication). A quality score of 3 means an excellent site and a quality weight of 1.00, Scores of 2 and 1 correspond to more problematic sites (linked to a complex local orography or instrument related problems) with corresponding quality weights of 0.67 and 0.33, respectively. Sites with quality score 0 are too problematic to be considered, including high-altitude mountain sites. The range score captures the ability of local statistics to represent properties in adjacent grid points. A score of 0 indicates that the site statistics only applies within a 100km range, thus it can affect only the local 1*1 grid point. Scores of 1, 2 and 3 indicate applications to 300, 500 and 900km, respectively, lending local statistics to surrounding grid-points.

2. place local AERONET statistics onto the regular horizontal grid of model median fields
Site information on quality and range is applied for AERONET re-gridding onto a regular 1*1 grid. First the quality score of a site is split onto the four adjacent grid-point centers based on the concept of inverse distance weights. If the range-score exceeds zero, then the fractional value at each of the four grid points is extended with an inverse grid-distance square weight ($1/\{1+[\Delta(lat)*\Delta(lat)+\Delta(lon)*\Delta(lon)]\}$) to the next neighbors for a range score of 1, to two layers of neighbors for a range score of 2 and to four-layers of neighbors for range scores of 3. As the monthly statistics of all AERONET sites is now processed (and if permitted also extended to surrounding pixels), at each grid point both weighted AERONET property and weight are accumulated (weight = [quality score] * [distance decay]). Their ratio defines at non-zero grid points a globally sparse monthly gridded fields (at model resolution) representing AERONET statistics.

3. define a global field of 'AERONET to model' ratios
For all non-zero elements of the gridded AERONET data, property ratios to the model median were determined. Each local ratio was spread over the surrounding +/- 180^o longitude and +/- 45^o latitude domain, where the local weight corresponding to AERONET quality score, decayed with increasing distance (weight = [quality weight] /[1.0+(distance/100km)]). Local ratios over continental sites were allowed only to contribute ratios over land surfaces, and similarly ratios contributions over ocean sites were only accepted from ocean sites. Once all available ratios were spread, then the weighted mean at each grid point (separately for each month) determined the global fields for 'AERONET to model' ratios.

4. establish 'weight-factor' fields by combining site associated weight factor domains
The quality and the range scores assigned to each AERONET site are used to determine local weight factors to be applied to 'AERONET to model' ratios. For each site, with a range score larger than zero, regional domains were defined, where circles (with a 1000km*range-score radius) were stretched in longitude by a factor 4. In addition, a cosine weight was introduced, which assured the domain was primarily stretched to the east at high mid-latitudes (ca 55^oN or S) and to the west at the equator to approximate prevailing winds. The local quality score linearly decreased to zero at the outer boundaries of the domain. When spreading the quality score of each site within its domain once again the separation between ocean and continental sites allowed only land contributions for land-sites and only ocean contributions for ocean sites. After all sites were processed, then at each location (and for each month) the largest weight at any location and month was picked to define the 'weight factor' fields.

5. establish 'effective weight factors' ('weight factor' times 'AERONET to model' ratios)
The 'AERONET to model' ratio fields were multiplied with the 'weight factor' fields to yield the 'effective weight factors'. To obtain the global fields of the new climatology, 'effective weight factor' fields are multiplied onto corresponding monthly fields of the model median.

For the three aerosol properties of 'aot', 'ssa' and 'An', the annual global fields of the model median, of the new climatology and of the AERONET local statistics are compared in Figures 2.

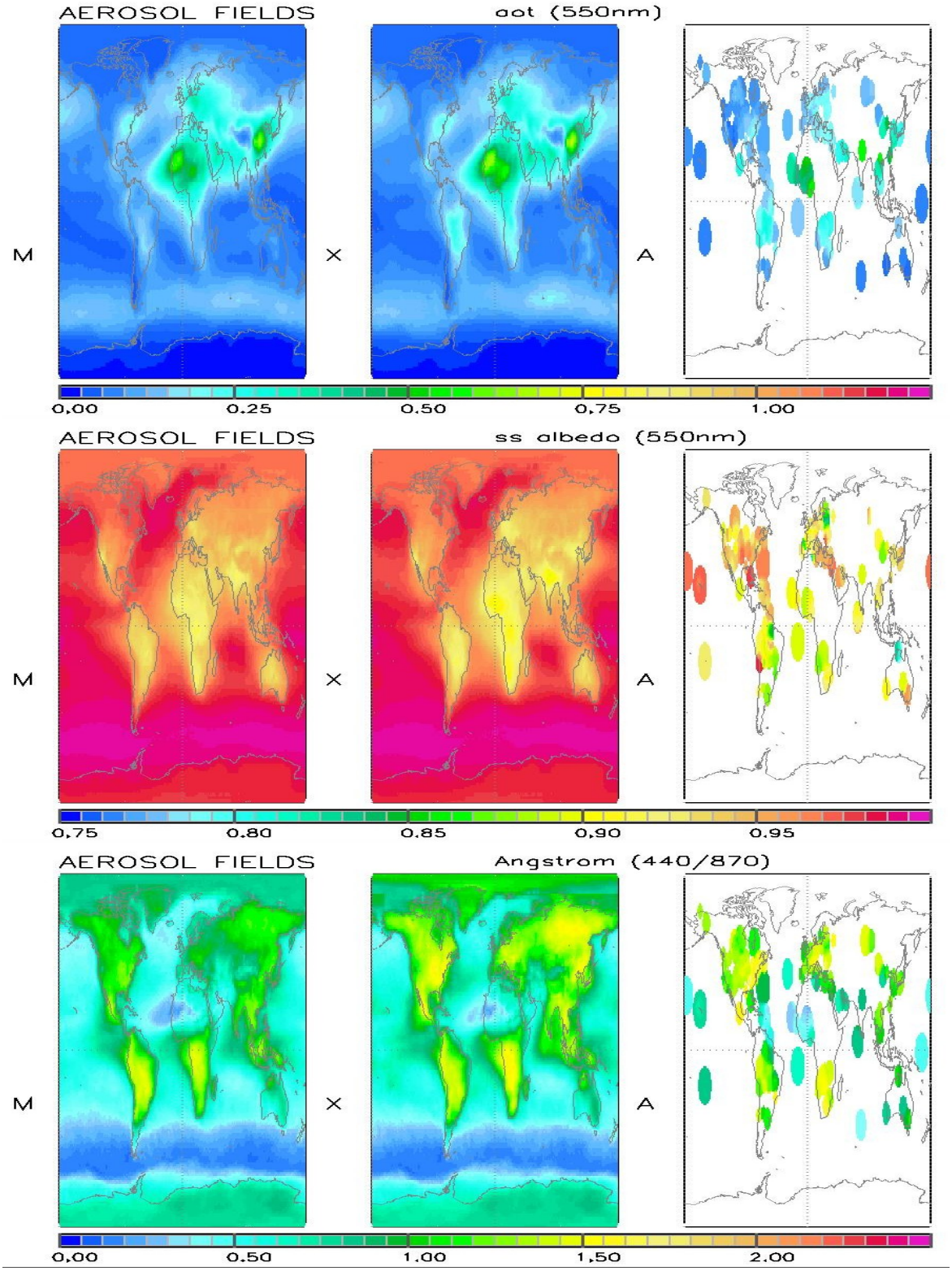

Figure 2. Annual average fields for the aerosol properties of the 'aot', 'ssa' and 'An' of the model median (M), the new climatology (X) and AERONET (A, *artificially enlarged*)

Figure 2 displays in its center panels the annual global fields of the new aerosol climatology at the mid-visible wavelength of 0.550μm. Radiative forcing is usually understood as the combined effect of impacts at all solar and infrared wavelengths. Thus, several assumptions were necessary to provide needed aerosol input at other than mid-visible wavelengths. In addition, also the derivation of 'g' from 'An' data was still needed.

1. 'aot'- and its spectral dependence

The absolute value for aot and its spectral dependence are provided by 'aot' and 'An'

2. 'ssa' – and its spectral dependence

The mid-visible value for 'ssa' is assumed constant for the entire solar region. The infrared radiative transfer is primarily influenced by larger particles of sea-salt and dust. Since elevated aerosol is of particular importance, dust aerosol properties were chosen to define the infrared values for 'ssa' and also 'g'. Here, the optical properties were based on a particle effective radius of 2 (log-normal (number-) size distribution with mode radius of 0.6μm and a standard deviation of 2) and characteristic refractive indices for dust (I.Sokolik, private communications).

3. 'g' – and its spectral dependence

AERONET based data-pairs for Angstrom parameter and associated asymmetry-factors in the ultra-violet, visible and near-IR (see Figure) were applied to derived a simple wavelength ('w') dependent relationship at solar wavelengths [g = 0.72 -0.14 * 'An' * ('w' -0.25)$^{0.5}$]. For the infrared region, as explained under 'ssa', the asymmetry-factors of dust were prescribed.

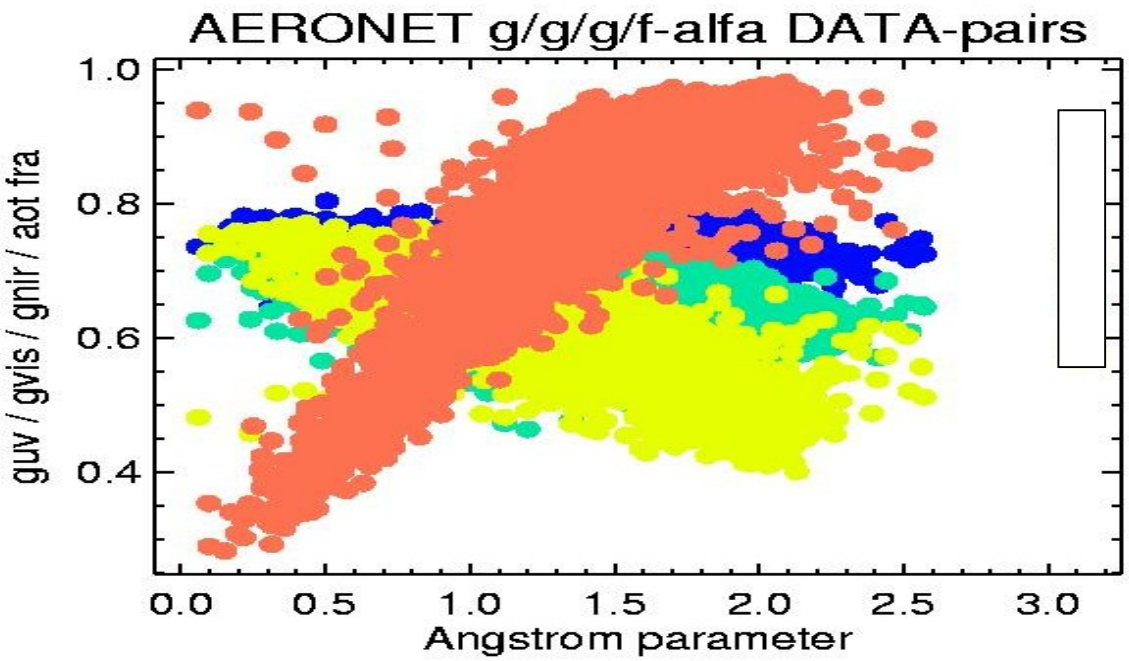

Figure 3. Scatter plots of AERONET data-pairs for between Angstrom parameter 'An' and asymmetry-factor 'g' in the UV (blue), in the visible (green) and in the near-IR (yellow). Also displayed (red) is the 'An' relationship to the aot-fraction of sizes smaller than 1μm.

Environmental properties

For environmental properties the model input relied on available data-sets. Satellite observations of the MODIS sensor define the solar surface albedo separately for the UV/visible (<0.69μm) and the n-IR (>0.69μm) spectral region (Schaaf .et al, 2002, see also Figure 4). Over oceans a multiplier $[(1.1*(\mu_0^{1.4}+0.15))^{-1}$, with μ_0 as the cosine of the solar zenith angle] accounted for increasingly larger solar albedos towards lower sun-elevations. For all-sky simulations necessary cloud properties are based on ISCCP statistics (Rossow et al., 1993). ISCCP supplies data on cloud cover at three altitude regimes ('low', 'mid' and 'high', see also Figure 5) and a regional average for the cloud optical depth. Assuming random cloud overlap, all-sky results are always based on eight (2^3) simulations, as each cloud-level combination is considered. In those simulations, cloud microphysics are based on standard size-distributions ('C1' $[r_{eff}=6\mu m]$, on 'C5' $[r_{eff}=10\mu m]$ and 'CS' $[r_{eff}=40um]$ for low-, mid- and high-level clouds). Cloud optical depths for each cloud layer are set by constraints of individual cloud cover, total scene cloud optical depth and an assumed fixed optical depth ratio of 5 (low) to 2 (mid) to 1 (high). Cloud layer altitude was set at 1-2km above ground, in at the center height of the troposphere and 1-3km below the tropopause, for low-, mid- and high level clouds, respectively. Profiles for temperature and trace-gases were selected (based on season and latitude) from (seven) standard atmospheric profiles (Andersen et al., 1986).

In the context of environmental properties (e.g. clouds, temperature and relative humidity) the aerosol altitude positioning becomes important. Aerosol vertical placement (see also Figure 6) was based on 'ECHAM5' (Roeckner et al., 2003) simulations with the HAM aerosol component module (Stier et al., 2005). Another data-set from modeling defines the anthropogenic fraction of the sub-micron size aerosol optical depth (see also Figure 4), as output from LOA (Reddy and Boucher, 2004) simulations with AeroCom emissions for years 1750 and 2000 were compared.

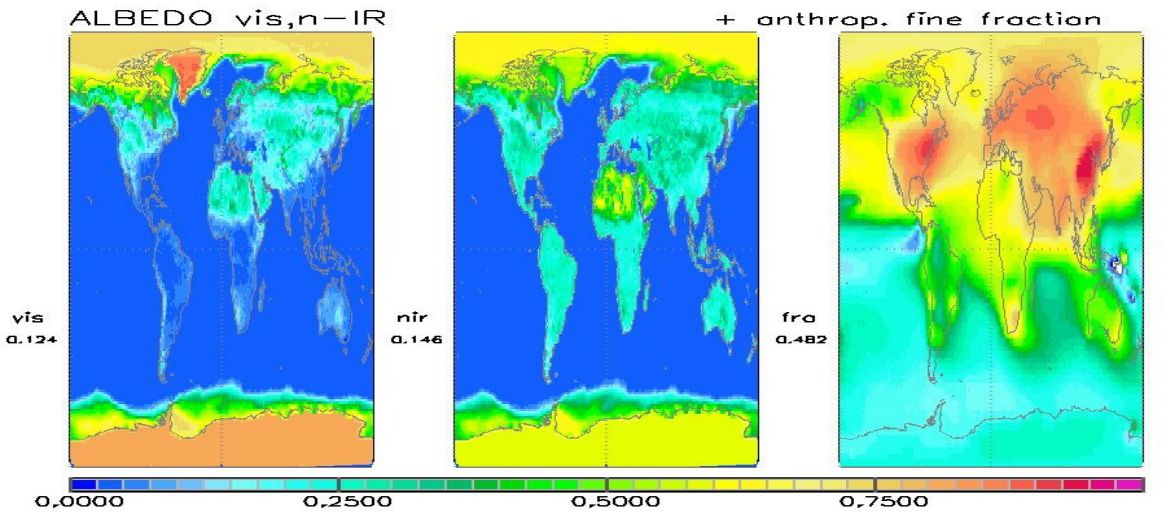

Figure 4. Annual average fields for solar surface albedo on the visible (vis) and in the near-infrared (nir) and the model simulated anthropogenic fraction for aerosol smaller than 1μm. Annual global field averages are also displayed.

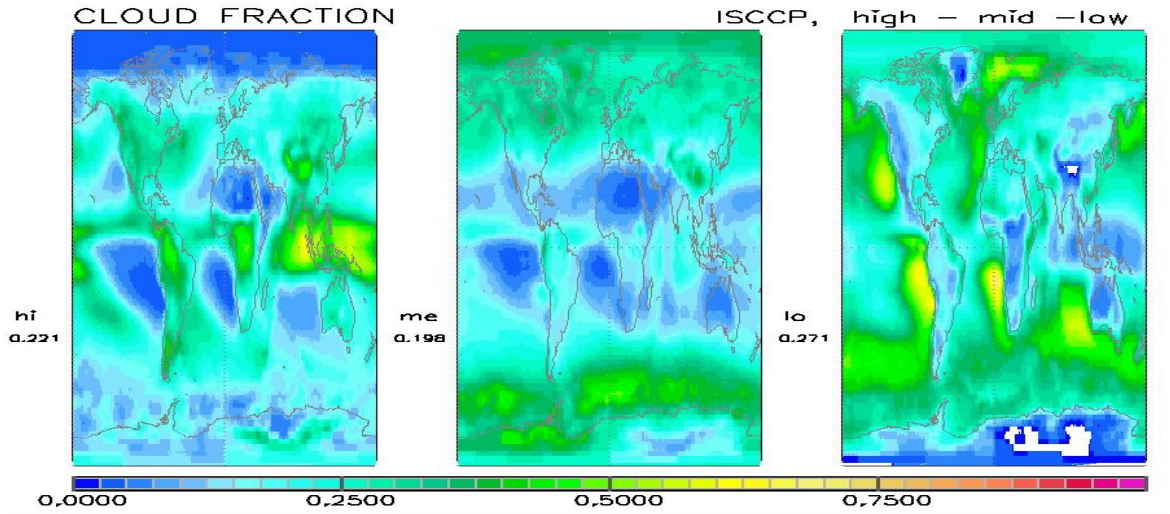

Figure 5. Annual average fields for ISCCP cloud cover for high altitude (hi), median altitude (me) and low altitude (lo) clouds. Annual global field averages are also displayed.

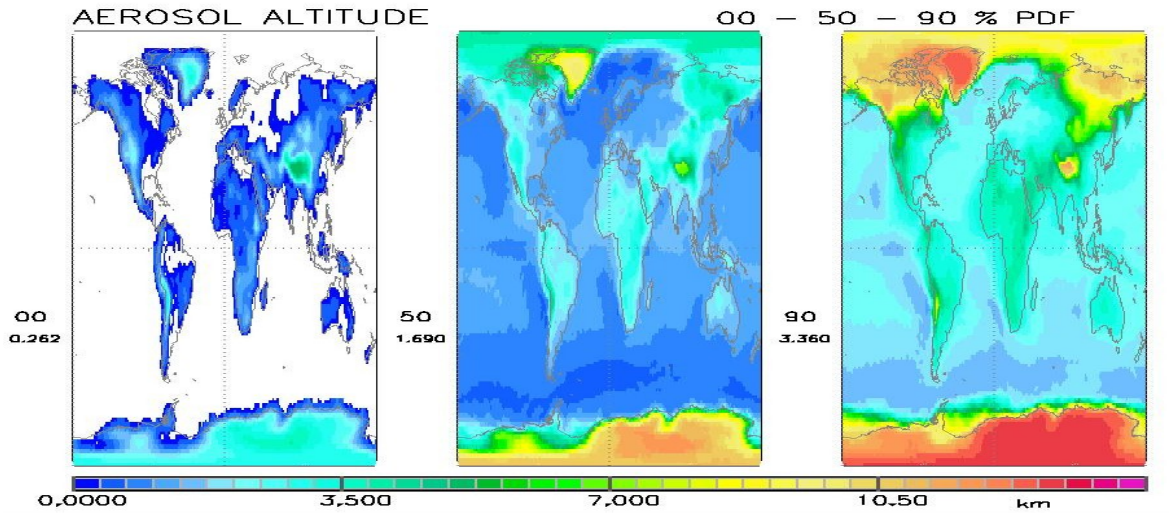

Figure 6. Annual average fields aerosol altitude PDF. PDF=0% (00) indicates the surface altitude, PDF=50% (50) displays the aerosol median height and PDF=90% (90) indicates the altitude below which 90% of the aot is located. Annual global field averages are also shown.

3. FORCING SIMULATIONS

Calculations of the radiative forcing are deduced from the difference of two broadband radiative transfer simulations, where everything is kept identical - except for the forcing agent (here aerosol). In this study, the broadband aspect is represented by the sum of simulations at 8 solar and 12 infrared spectral sub-regions, thereby assuming that optical properties of atmospheric particles within each sub-region can be characterized by one simulation at its central wavelength (of course, times the number of necessary exponential terms to represent the absorption by atmospheric trace-gases).

Clear-sky (no-cloud) forcing and forcing efficiencies (forcing per unit 'aot') at the top of the atmosphere (upper figure) and at the surface (lower figure) are compared among model median, new climatology and AERONET (in the format of Figure 2) in Figures 7 to 10.

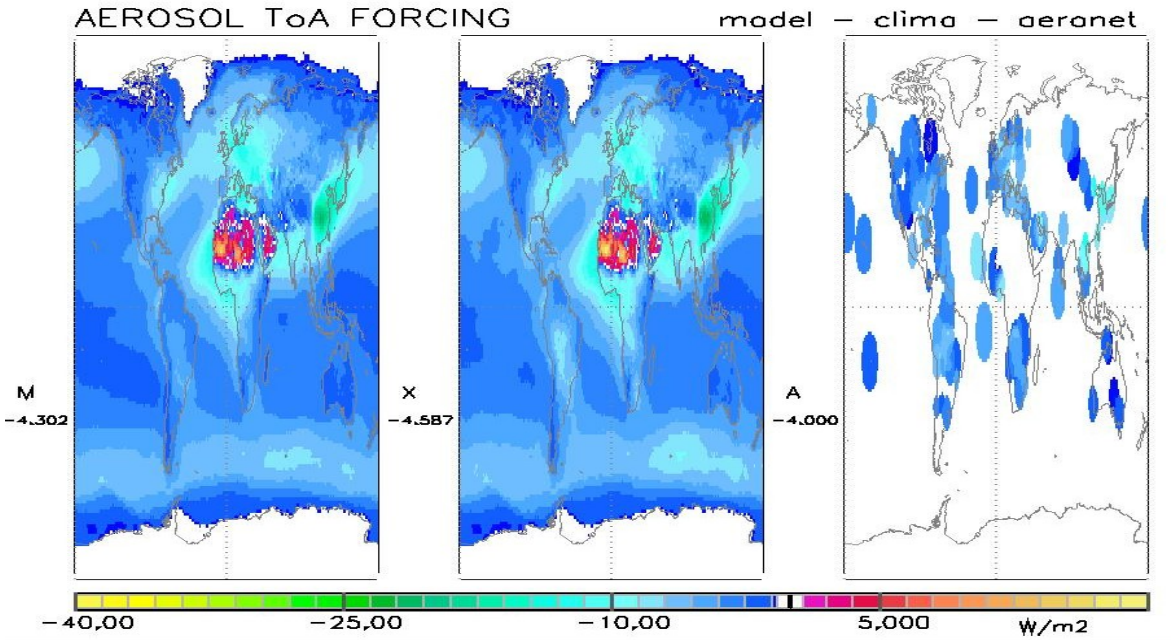

Figure 7. Annual average fields for the aerosol direct clear-sky radiative forcing at ToA attributed to model median (M), new climatology (X) and AERONET (A, *artificially enlarged*)

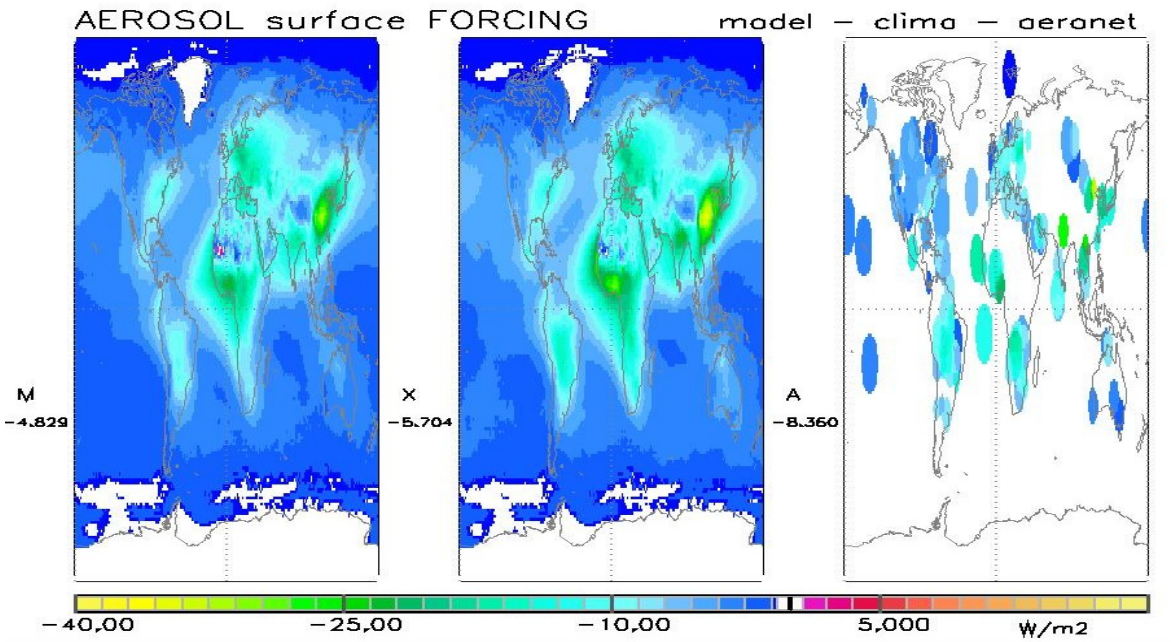

Figure 8. Annual average fields for the aerosol direct clear-sky radiative forcing at ground attributed to model median (M), new climatology (X) and AERONET (A, *artificially enlarged*)

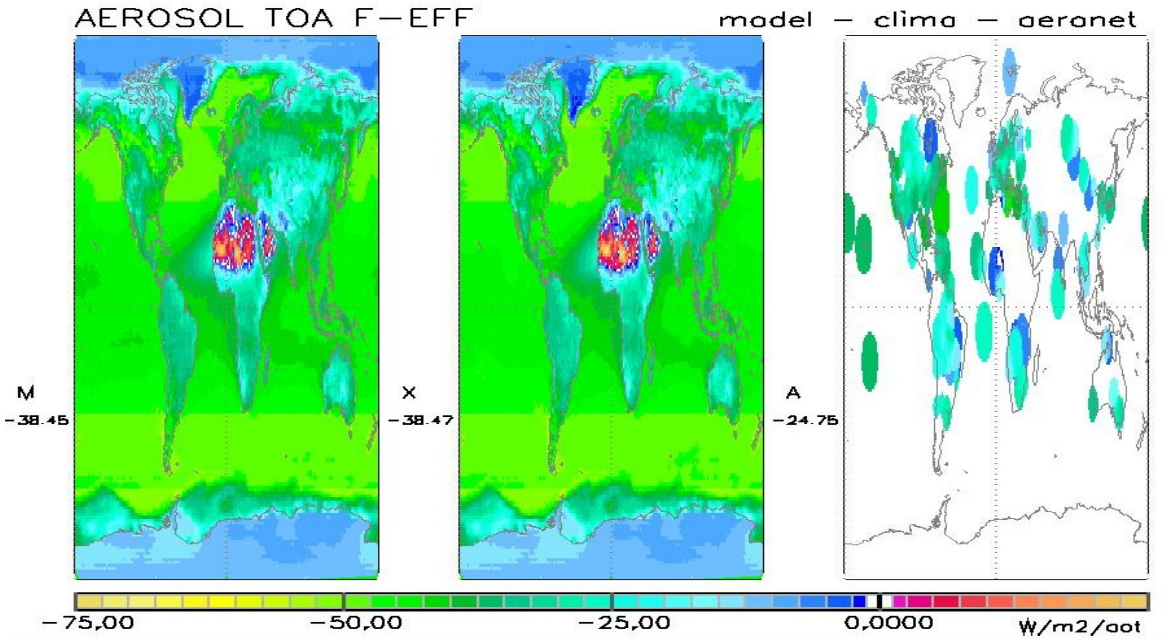

Figure 9. Annual average fields for the aerosol direct clear-sky radiative forcing efficiency (= forcing per unit aot) at ToA attributed to model median (M), new climatology (X) and AERONET (A, *artificially enlarged*)

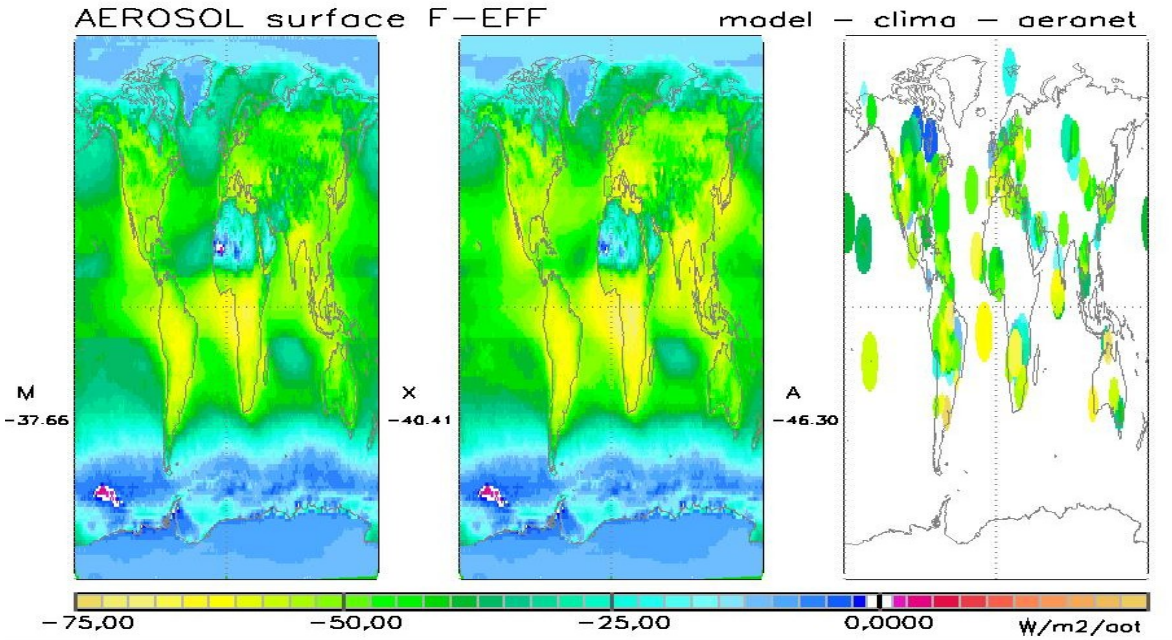

Figure 10. Annual average fields for the aerosol direct clear-sky radiative forcing efficiency (= forcing per unit aot) at the surface attributed to model median (M), new climatology (X) and AERONET (A, *artificially enlarged*)

Forcing results are calculated for solar and infrared spectral regions (subsequently shown is the combined total), for both clear-sky and cloudy conditions and for both total (the new climatology) and anthropogenic aerosol. Here, anthropogenic aerosol contributions are assumed to be associated with sub-micron size particles only. For these smaller aerosol sizes, the solar extinction (absorption and scattering) is much stronger than in the infrared. Thus, for 'ssa' and 'g' the infrared selections are only of minor importance and only the assumptions defining the solar choices are discussed.

1. anthropogenic aot

AERONET based data-pairs for Angstrom parameter and small mode aot fraction (see also Figure 2) establish a simple relationship [f = 0.19 + 0.687* ln('An' +1), for -0.15<'An'<2.25]. After the separation into super- and sub-micron sizes, the Angstrom parameter of the smaller size is determined by assuming that the aot fraction attributed to the larger aerosol sizes has no spectral dependence. The absolute value for 'aot' is defined by the product of small (size) mode aot fraction and an anthropogenic factor, (see Figure 3) based on the comparison of model-simulations with emission scenarios for the years 2000 and 1750. The Angstrom parameter associated with smaller sizes defines the anthropogenic aot spectral dependence.

2. anthropogenic 'ssa'

With separations into aots fractions linked to larger and smaller sizes, it is assumed that the aot of the smaller sizes have twice the absorption strength (1-'ssa') of larger sizes. The mid-visible 'ssa' attributed to the smaller sizes applies at all solar wavelengths.

3. anthropogenic 'g'

Based on the AERONET-Angstrom relationship [g = 0.72 -0.14 * 'An_L' * ('w' -0.25)$^{0.5}$], now the Angstrom parameter associated with the smaller sizes is applied.

Changes to the radiative energy balance are examined specifically at the top of the atmosphere (ToA) to summarize the overall impact on climate and at the surface to address the impact on surface processes. A sample comparing the annual global fields of the different simulated aerosol direct radiative forcings is given in Figure 11. For a quick comparison, the global annual averages are also listed in Table 1. Table 1 also demonstrates that (at least on a global scale) interactions at solar wavelength dominate the aerosol direct forcing.

Complementary, for the aerosol forcing efficiency, the aerosol forcing per unit optical depth, results with the new aerosol climatology are presented in Figure 12 and Table 2.

Table 1. Comparison of annual global calculated aerosol forcings based on the AERONET/AeroCom new aerosol climatology

Forcing (W/m^2)	total	(solar+IR)	solar	(only)
	clear-sky	ISCCP	clear-sky	ISCCP
at Top of Atmosphere	**- 4.6**	**- 2.7**	**- 5.0**	**- 2.9**
at surface	**- 5.7**	**- 4.3**	**- 7.3**	**- 5.2**
at ToA, anthropogenic	**- 1.6**	**- 1.0**	**- 1.7**	**- 1.0**
at surface, anthropogenic	**- 2.7**	**- 2.0**	**- 2.8**	**- 2.1**

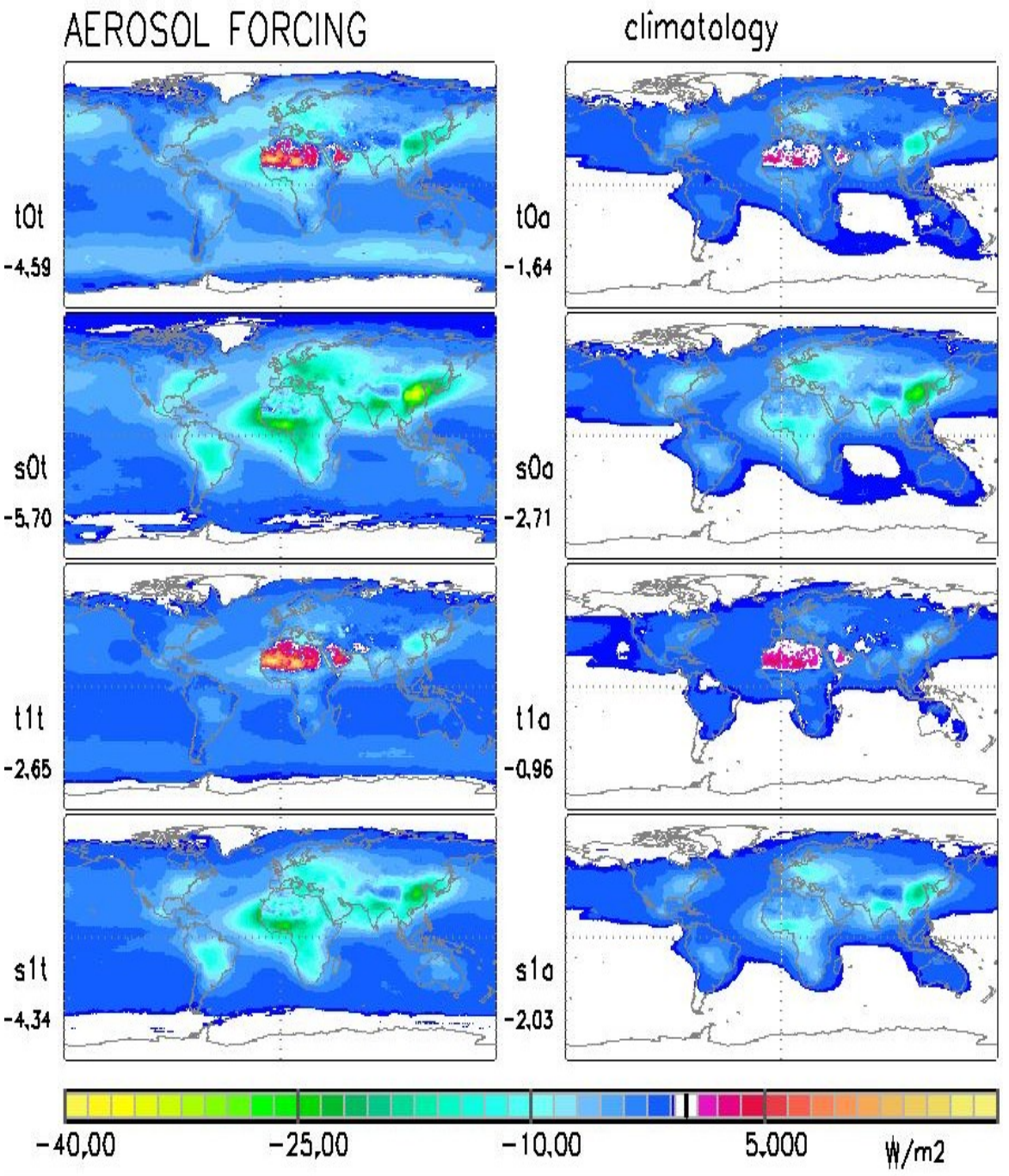

Figure 11. Aerosol forcing associated with the new aerosol climatology. Left panels show results for total (natural and anthropogenic) aerosol. Results for anthropogenic aerosol only are displayed in the right panels. The upper two rows display clear-sky results (0), while the lower two rows display results for all-sky conditions (1). First and third rows show simulated ToA forcing fields, whereas second and fourth rows display surface forcing results. Indicated as well are global annual averages. (Monthly fields for 't1a' and 's1t' are in the Appendix)

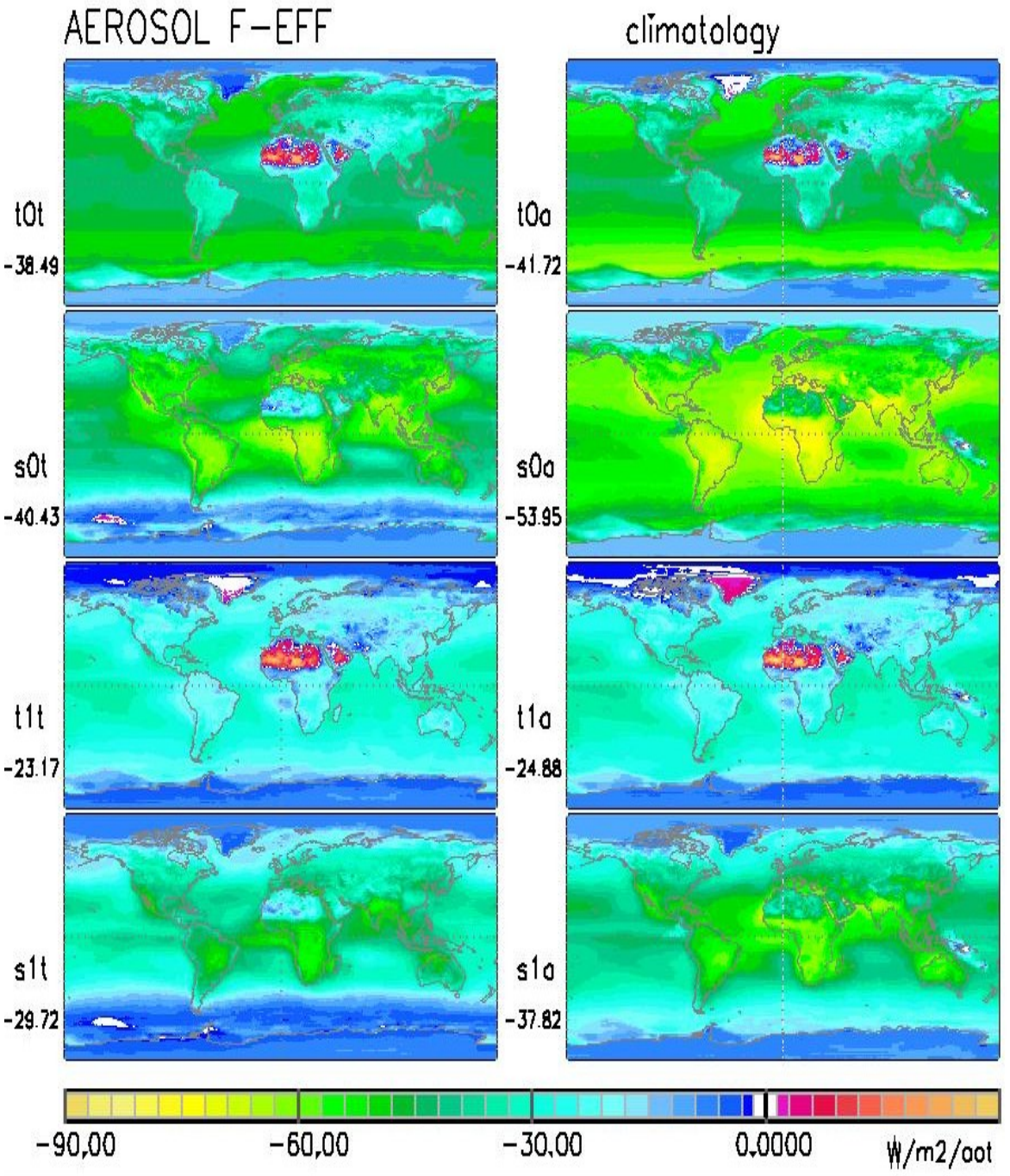

Figure 12. Aerosol forcing efficiency associated with the new aerosol climatology. Left panels show results for total (natural and anthropogenic) aerosol. Results for anthropogenic aerosol only are displayed in the right panels (referring to anthropogenic aot). The upper two rows display clear-sky results (0), while the lower two rows display results for all-sky conditions (1). First and third rows show simulated ToA forcing fields, whereas second and fourth rows display surface forcing results. Indicated as well are global annual averages.

Table 2. Comparison of annual global aerosol forcing efficiencies based on the new (AERONET/AeroCom) aerosol climatology

F - Efficiency (W/m^2 / aot)	total	(solar+IR)	solar	(only)
	clear-sky	ISCCP	clear-sky	ISCCP
at Top of Atmosphere	**- 38**	**- 23**	**- 41**	**- 25**
at surface	**- 40**	**- 30**	**- 53**	**- 36**
at ToA, anthropogenic	**- 42**	**- 25**	**- 42**	**- 25**
at surface, anthropogenic	**- 54**	**- 38**	**- 56**	**- 39**

Forcing efficiency include all information on environmental and all aerosol properties - except aot. Thus, this property is rather convenient to trying to asscociate forcing to satellite retrievals, which can only determine aot fields with some skill. Applications to various aot remote sensing data-satellite aot data sets are illustrated in Figure 13.

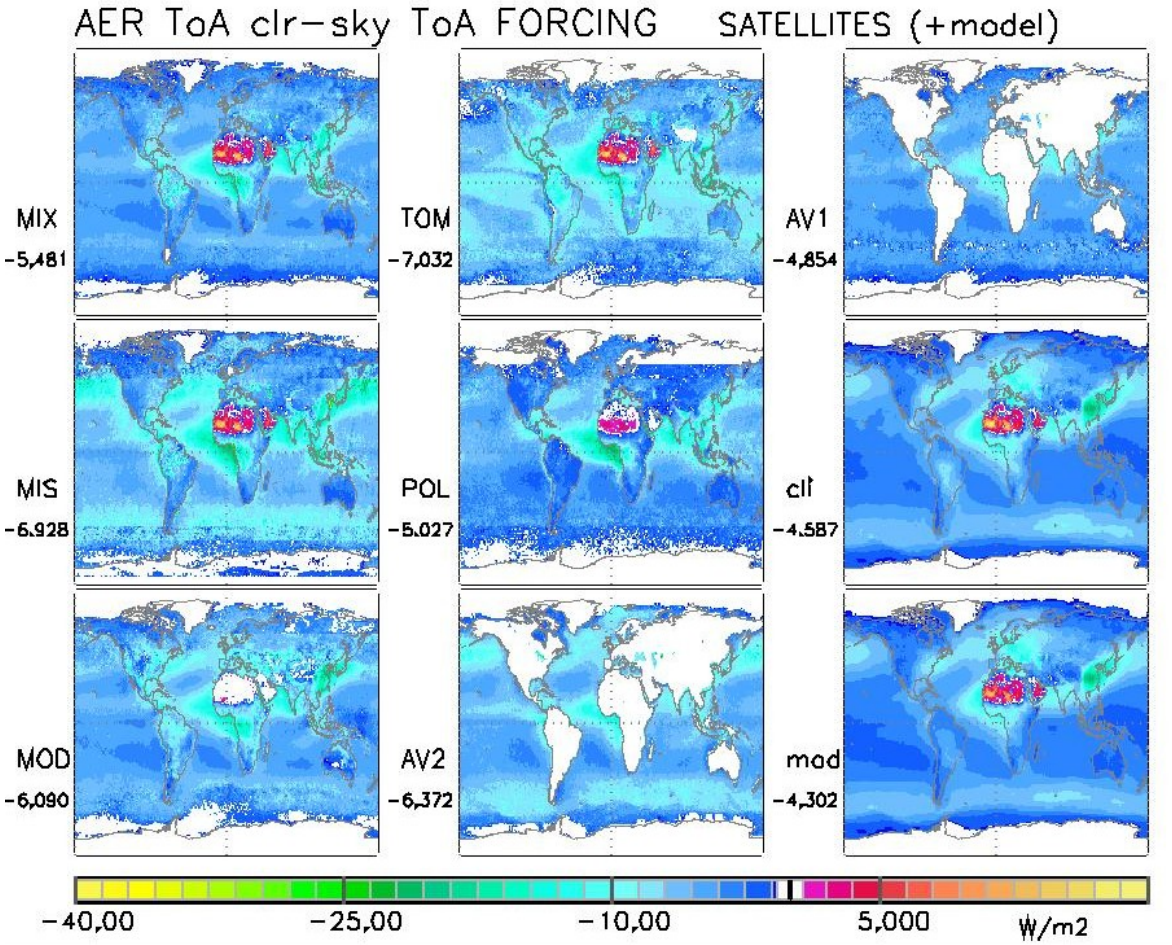

Figure 13. Aerosol forcing linked to different multi-year satellite aot data sets are compared to forcings with the climatology (cli) and the model median (mod) MIX:Figure 1 composite, MISR-, MODIS-, TOMS-, POLDER-, AVHRR, 1channel-, AVHRR, 2channel retrievals

3. DISCUSSION

The radiative transfer simulations with the new aerosol climatology can be summarized in a few numbers:

ca - 5 W/m^2	the globally averaged clear-sky ToA cooling (agrees with CERES estimates)
ca 2/3	factor applied to clear-sky forcing to yield all-sky forcing
ca 1/3	factor applied to total forcing to yield anthropogenic forcing - globally
ca 2/3	factor applied to total forcing to yield anthr. f. - for industry regions of NH
ca 5/3	factor applied to ToA forcing to yield surface forcing
ca 1/10	IR to solar forcing ratio at ToA (IR warming partially offsets solar cooling)
ca 1/4	IR to solar forcing ratio at surface (IR warming partially offsets solar cooling)
➔ - 1 W/m^2	the globally averaged ToA anthropogenic direct (all-sky) aerosol forcing (this value is comparable to **2.4 W/m^2** warming by anthr. greenhouse gases)

The calculated anthropogenic cooling for aerosol forcing is significant larger than suggested by global modeling (compare **- 1 W/m^2** of the climatology to **– 0.2 W/m^2** as typical value in global modeling). It is most likely that these difference are associated with differences in the presence of clouds, aerosol-cloud interactions not considered in our simulations and differences in the relative altitude placement between aerosol and clouds. Simulations of the total (natural and anthropogenic) clear-sky direct aerosol forcing are probably more meaningful, as they require fewer assumptions to environmental properties. A comparison of global annual averages is given in Figure 14.

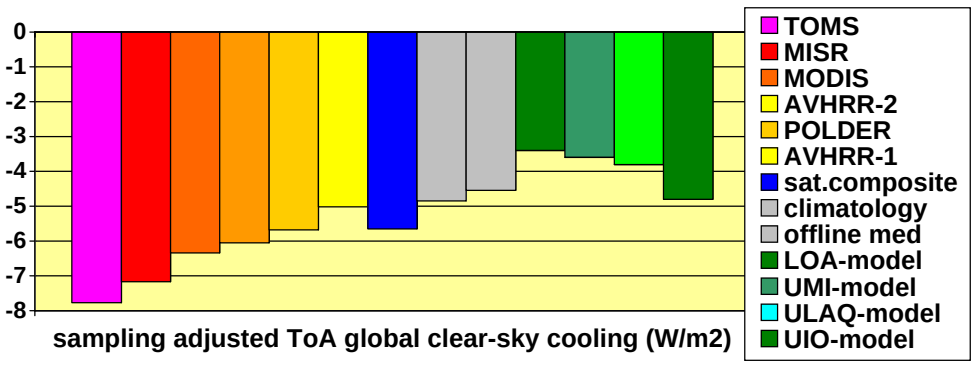

Figure 14. Global annual averages for the clear-sky direct aerosol forcing at the ToA. Satellite data were sample adjusted with the climatology (note, ToA cooling associated with satellite data in excess of -7W/m2 can be attributed to known aot overestimates of retrievals) Model estimates are provided via the AeroCom activity (M. Schulz, private communication)

The suggested ToA cooling is just between lower value suggested by global modeling and larger value suggested by satellite data (when combining retrieved aot-fields with the forcing efficiency of the climatology.

In order to understand, how the new aerosol climatology matches up with detailed local calculation at AERONET sites, the calculated forcings of the new aerosol climatology are locally sub-sampled at site and months, when AERONET based forcing could be provided. Global averages for forcing and forcing efficiency are compared in Tables 3 and 4.

Table 3. Comparison of annual aerosol forcings only at AERONET sites applying AERONET-detail (size, absorption) 'Aer' and using the new aerosol climatology 'clim'

Forcing (W/m^2)	tot	-clr		tot	-cld		sol	-clr		sol	-cld
	Aer	clim		Aer	clim		Aer	clim		Aer	clim
at Top of Atmosphere	**- 6.7**	**- 4.5**		**- 4.1**	**- 2.7**		**- 7.2**	**- 4.9**		**- 4.4**	**- 3.0**
at surface	**-11.5**	**- 9.5**		**- 9.1**	**- 7.8**		**-12.7**	**-11.0**		**- 9.6**	**- 8.8**

Table 4. Comparison of annual aerosol forcing efficiencies only at AERONET sites applying AERONET-detail (size, absorption) 'Aer' and using the new aerosol climatology 'clim'

Forcing Eff. (W/m^2 /aot)	tot	-clr		tot	-cld		sol	-clr		sol	-cld
	Aer	clim		Aer	clim		Aer	clim		Aer	clim
at Top of Atmosphere	**- 38**	**- 29**		**- 24**	**- 17**		**- 40**	**- 31**		**- 25**	**- 19**
at surface	**- 56**	**- 54**		**- 43**	**- 44**		**- 61**	**- 63**		**- 46**	**- 50**

The forcing of the new climatology is less negative both at the surface and at the top of the atmosphere. While the atmospheric forcing (solar ToA forcing – solar surface forcing) is generally well reproduced, the ToA forcing efficiency of the climatology is clearly lower. This suggests that in the new climatology the aot is underestimated and the solar absorption is overestimated compared.

There is clearly potential to improve on this initial effort of a new aerosol climatology. New and more quality data, not just limited to AERONET are now becoming available and these will certainly lead to improved aerosol fields and associated forcings. Nonetheless, this initial effort already provided a general reference for the global distribution of important aerosol properties.

Acknowledgements

Support by the German Weather Service and the European GEMS project for the effort is acknowledged. The AeroCom (http://nansen.ipsl.jussieu.fr/AEROCOM) global modeling effort was essential to this study, as the (16) model median provides the starting point for the new aerosol climatology. Thus the work of all global modeling groups that contributed to AeroCom is particular acknowledged. Important data were provided many satellite retrievals groups of the US and certainly by the AERONET group at NASA-GSFC, with particular help and input from T.Eck and D.Giles.

References

Anderson, G., S.Clough, F.Kneizys, J.Chetwynd, E. Shettle, AFGL Atmospheric Constituent Profiles (0.120km), *Air Force Geophysics Lab Hanscom AFB, MA, Report A371571*, 1986.

Holben, B., T.Eck, I.Slutsker, D.Tanre, J.Buis, E.Vermote, J.Reagan, Y.Kaufman, T.Nakajima, F.Lavenau, I.Jankowiak and A.Smirnov, AERONET, a federated instrument network and data-archive for aerosol characterization, *Rem.Sens.Environ. 66*, 1-66, 1998.

S.Kinne, M.Schulz, C.Textor, S.Guibert, S.Bauer, T.Berntsen, T.Berglen, O.Boucher, M.Chin, W.Collins, F.Dentener, T.Diehl, R.Easter, J.Feichter, D.Fillmore, S. Ghan, P.Ginoux, S.Gong, A.Grini, J.Hendricks, M.Herzog, L.Horowitz, I.Isaksen, T.Iversen, D.Koch, M.Krol, A.Lauer, J.F.Lamarque[8], G.Lesins, X.Liu, U.Lohmann, V.Montanaro, G.Myhre, J.Penner, G.Pitari, S.Reddy, O.Seland, P.Stier, T.Takemura, X.Tie, An AeroCom initial assessment – optical properties in aerosol component modules of global models, *accepted in ACP* 2005

Reddy, M. S., and O. Boucher, A study of the global cycle of carbonaceous aerosols in the LMDZT general circulation model, *Journal of Geophysical Research*, 109(D14), D14202, doi:10.1029/2003JD004048, 2004.

Roeckner, E. G.Baeml, L.Bonaventura, R.Brokopf, M.Esch, M.Giorgetta, S.Hagemann, I.Kircher, L.Kornblueh, E.Manzini, A.Rhodin, U.Schlese, U.Schulzweida, A.Tomkins; The atmospheric general circulation model ECHAM5, *MPI-Reports 349 and 354*, 2003.

Rossow, W., A.Walker and C.Garder, Comparison of ISCCP and other cloud amounts, *J.Climate 6* 2394-2418, 1993.

Schaaf, C., F.Gao, A.Strahler, W.Lucht, X.Li, T.Trang, N.Strucknell, X.Zhang, Y.Jin, J.-P.Mueller, P.Lewis, M.Barnsley, P.Hobson, M.Disney, G.Roberts, M.Dunderdale, R.D'Entremont, B.Hu, S.Liang, J.Privette and D.Roy. First oberservational BRDF, albedo and nadir reflectance from MODIS, *Remote Sens. Environ., 83*, 135-148, 2002.

Stier P., J. Feichter, S. Kinne, S. Kloster, E. Vignati, J. Wilson, L. Ganzeveld, I. Tegen, M. Werner, M. Schulz, Y. Balkanski, O. Boucher, A. Minikin, A. Petzold, The aerosol-climate model ECHAM5-HAM *Atmospheric Chemistry and Physics 5*, 1125-1156, 2005.

Appendix

The Appendix list in Table A1 all AERONET sites which contributed to the new aerosol climatology along with site assigned scores for quality and range. In addition, in several Figures monthly distribution fields for a few important aerosol associated properties are presented:

'**s1t**' **s**_urface forcing under all-sky conditions (**1**) for the **t**_otal aerosol (natural +anthrop)
'**t1a**' **t**_op of atmsophere forcing under all-sky conditions (**1**) for **a**_nthropogenic aerosol

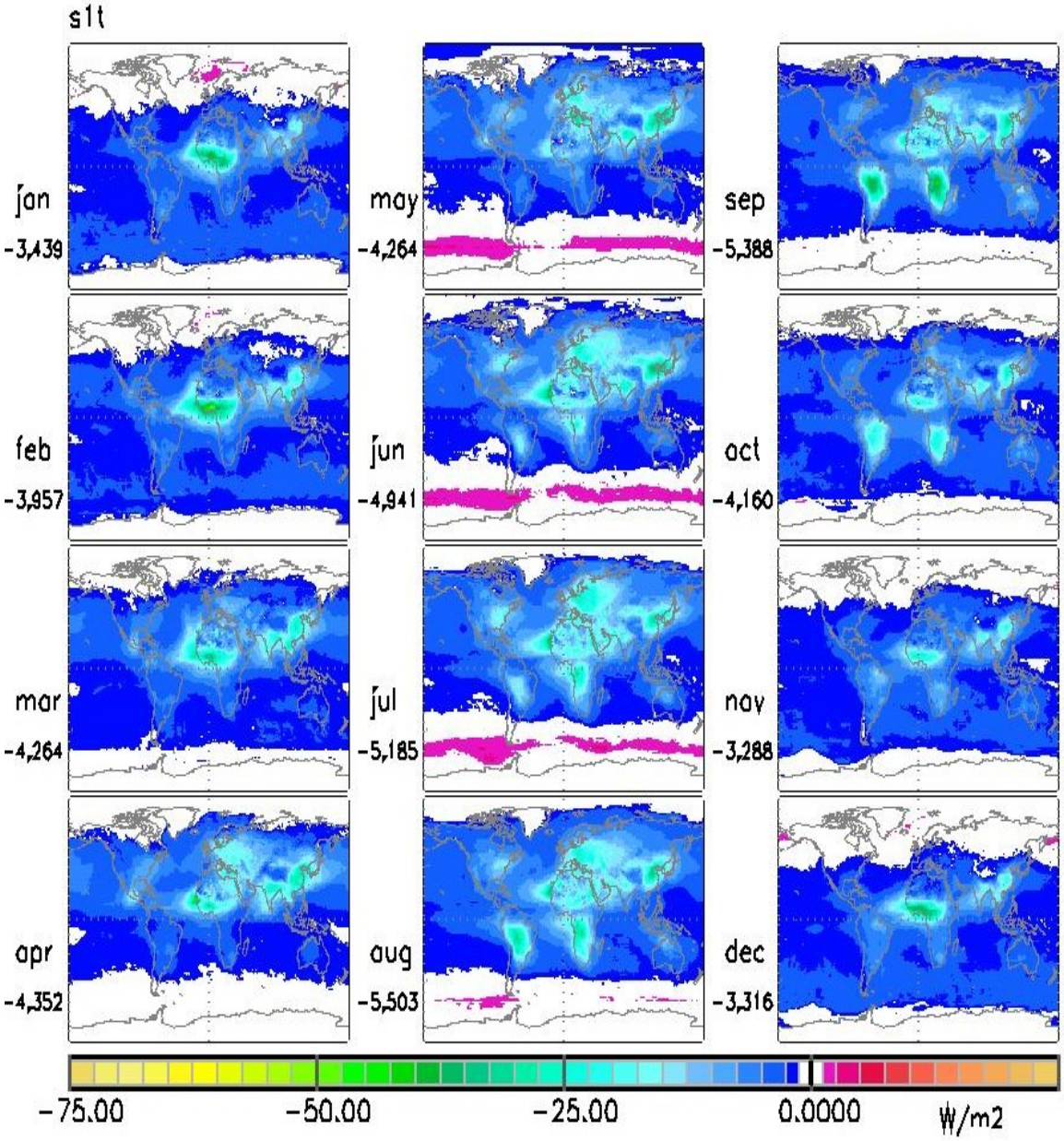

Figure A1. Monthly all-sky aerosol surface forcing. Also global averages are indicated.

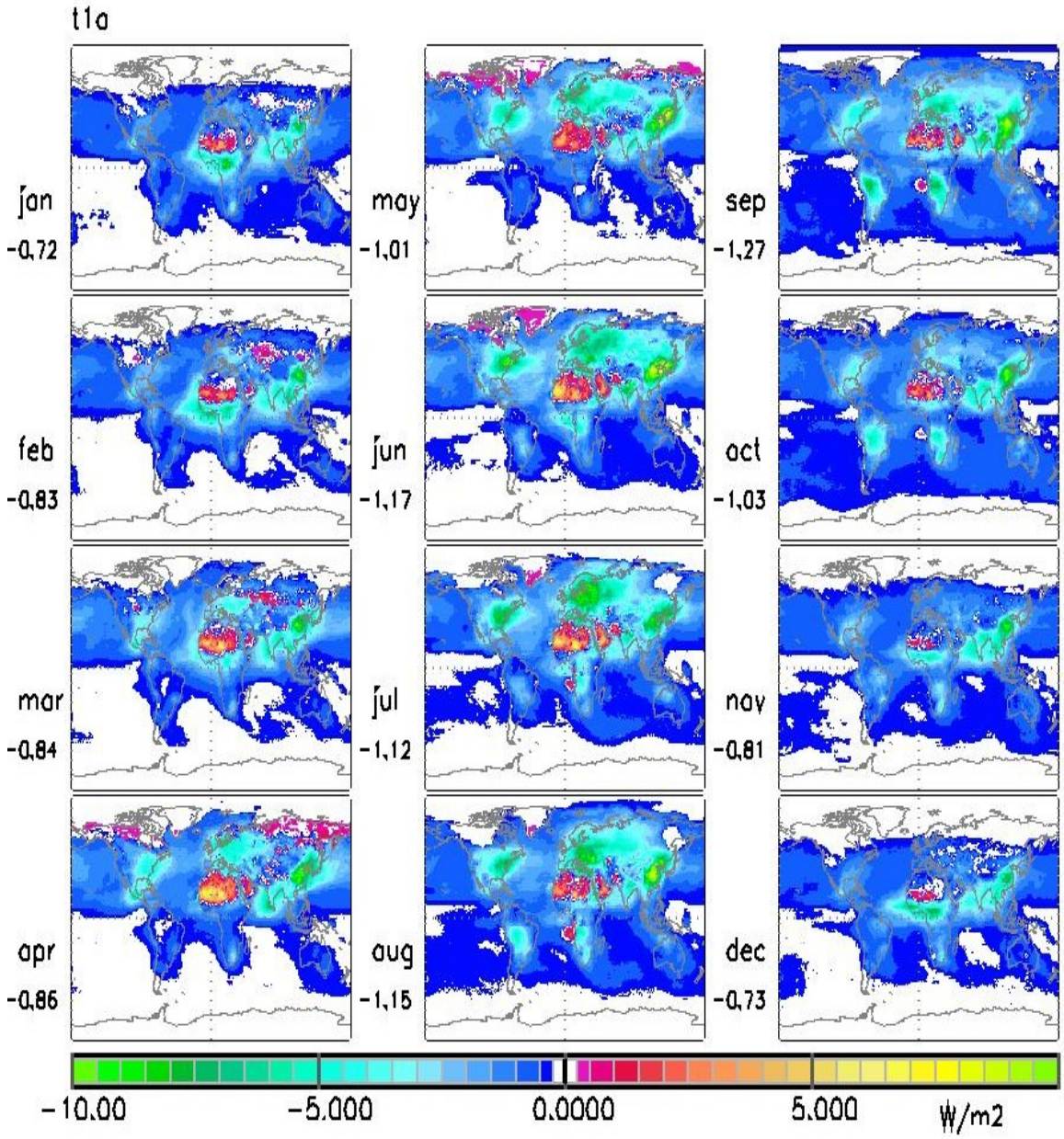

Figure A2. Monthly all-sky anthropogenic aerosol forcing at the top of the atmosphere. Also indicated are global averages on a monthly basis

Table A1. AERONET-sites: location, altitude, quality score (q) and range score (r)

lon(E)	lat(N)	z(m)	q	r	AERONET-site
-62.37	-10.77	200	3	1	Abracos_Hill
-1.48	15.35	305	3	2	Agoufou
-47.67	-15.58	1100	3	0	Aguas_Emendadas
-3.23	37.12	2103	0	0	Ahi_De_Cara
0.25	43.70	80	3	0	Aire_Adour
54.55	24.25	40	3	1	Al_Dhafra
55.10	24.17	192	3	1	Al_Khaznah
53.03	24.13	5	3	1	Al_Qlaa
-123.07	44.58	67	0	0	Albany_Oregon
-56.02	-9.92	175	3	1	Alta_Floresta
77.57	-37.82	30	3	2	Amsterdam_Island
16.02	69.28	379	3	0	Andenes
-77.80	24.70	0	3	1	Andros_Island
-119.53	35.95	210	3	0	Angiola
126.18	36.32	47	3	1	Anmyon
-70.32	-18.47	25	3	1	Arica
-3.23	37.13	691	0	0	Armilla
-14.42	-7.98	30	2	3	Ascension_Island
4.88	43.93	32	3	0	Avignon
-28.63	38.53	50	3	2	Azores
-88.37	40.05	212	3	1	BONDVILLE
-0.58	44.78	40	3	0	BORDEAUX
-105.02	40.03	1604	3	0	BSRN_BAO_Boulder
106.23	21.28	15	3	0	Bac_Giang
105.73	9.28	10	3	1	Bac_Lieu
50.50	26.33	0	3	1	Bahrain
-59.48	-1.92	80	2	2	Balbina
2.67	13.53	250	3	1	Banizoumbou
-59.50	13.17	0	2	1	Barbados
-156.67	71.32	0	2	0	Barrow
116.38	39.98	92	3	0	Beijing
20.78	51.83	190	3	0	Belsk
-54.95	-2.65	70	3	1	Belterra
-64.70	32.37	10	3	3	Bermuda
28.33	-28.25	1709	3	1	Bethlehem
-1.55	43.48	0	3	0	Biarritz
-2.45	14.07	0	3	2	Bidi_Bahn
-78.43	38.52	1082	0	0	Big_Meadows
-71.25	42.52	0	3	0	Billerica
-148.32	64.73	150	3	1	Bonanza_Creek
-3.75	11.85	0	3	2	Bondoukoui
-119.67	45.82	200	0	0	Bordman

-105.25	40.02	1600	3	0	Boulder
-47.90	-15.92	1100	3	1	Brasilia
-104.70	50.28	586	3	1	Bratts_Lake
-72.88	40.87	33	3	0	Brookhaven
26.52	44.45	44	3	0	Bucarest
-76.93	39.10	50	2	0	Burtonsville
-105.27	53.73	503	3	1	CANDLE_LAKE
-71.93	45.38	300	3	1	CARTEL
-97.42	36.62	315	3	1	CART_SITE
-73.95	40.82	100	3	0	CCNY
-58.50	-34.57	10	3	1	CEILAP-BA
-75.72	36.90	37	3	0	COVE
-80.42	25.65	5	3	1	CRYSTAL_FACE
-56.02	-15.73	210	3	1	CUIABA-MIRANDA
4.93	51.97	-1	3	0	Cabauw
-9.05	38.78	140	3	0	Cabo_da_Roca
-54.62	-20.45	500	3	1	Campo_Grande
149.12	-35.27	600	3	0	Canberra
-22.93	16.73	60	3	2	Capo_Verde
-104.23	32.37	942	3	1	Carlsbad
-97.42	36.62	315	3	1	Cart_Site
-71.93	45.38	300	3	0	Cartel_X
126.17	33.28	0	3	1	Che-Ju
120.22	23.00	50	3	0	Chen-Kung_Univ
-90.25	45.93	0	3	1	Chequamegon
-75.43	37.27	0	3	0	Cheritan
-117.75	35.67	800	3	0	China_Lake
128.65	35.17	69	3	0	Chinhae
100.53	13.73	115	3	0	Chulalongkorn
-93.82	58.73	10	3	2	Churchill
2.97	45.77	1464	3	0	Clermont_Ferrand
-157.78	21.43	0	1	1	Coconut_Island
146.07	-34.82	127	2	1	Coleambally
-81.03	34.02	104	3	0	Columbia_SC
-62.03	-16.13	500	3	1	Concepcion
-119.57	36.10	110	3	0	Corcoran
-64.47	-31.52	730	3	0	Cordoba-CETT
2.43	48.78	57	3	0	Creteil
-56.00	-15.50	250	3	1	Cuiaba
-15.95	23.72	12	3	1	Dahkla
-16.97	14.38	0	3	1	Dakar
104.42	43.58	1470	3	1	Dalanzadgad
130.88	-12.42	29	3	1	Darwin
35.45	31.10	-410	3	0	Dead_Sea
74.98	15.43	700	3	1	Dharwar

116.07	20.70	5	3	1	Dongsha_Island
-82.80	24.60	0	3	1	Dry_Tortugas
94.78	40.03	1300	3	1	Dunhuang
-75.75	36.18	0	3	0	EOPACE1
-75.75	36.18	0	3	0	EOPACE2
15.02	37.62	736	0	0	ETNA
-79.75	44.23	264	3	0	Egbert
-6.73	37.10	0	3	0	El_Arenosillo
-62.03	-14.77	225	3	1	El_Refugio
15.92	-19.17	1131	3	1	Etosha_Pan
-7.92	38.57	293	3	0	Evora
-101.68	54.67	305	3	1	FLIN_FLON
25.28	35.33	20	3	1	FORTH_CRETE
2.68	48.42	85	3	0	Fontainebleau
-119.77	36.78	0	3	0	Fresno
-73.97	40.80	50	3	0	GISS
73.82	15.45	20	3	1	GOA_INDIA
-76.88	39.03	50	3	1	GSFC
-77.22	39.13	50	3	1	Gaithersburg
13.92	46.68	1900	3	0	Gerlitzen
18.95	57.92	10	3	0	Gotland
-61.50	16.33	0	2	2	Guadeloup
-122.22	44.23	830	3	0	HJAndrews
-77.72	39.72	200	3	0	Hagerstown
-63.58	44.63	65	3	1	Halifax
9.97	53.57	105	3	0	Hamburg
-76.45	36.78	10	3	0	Hampton_Roads
-72.18	42.53	322	3	0	Harvard_Forest
7.88	54.18	33	3	1	Helgoland
-110.97	29.08	237	3	0	Hermosillo
-75.70	37.42	50	3	0	Hog_Island
-68.73	45.20	100	3	1	Howland
99.95	12.63	1	3	0	Hua_Hin
12.43	51.35	125	3	1	IFT-Leipzig
-100.62	36.57	850	3	1	IHOP-Homestead
8.50	39.92	10	3	0	IMC_Oristano
34.27	36.57	3	3	0	IMS-METU-ERDEMLI
12.33	45.43	20	3	0	ISDGM_CNR
4.33	8.32	350	3	1	Ilorin
32.90	-26.03	73	3	0	Inhaca
115.95	42.68	1343	3	1	Inner_Mongolia
103.08	51.80	670	3	0	Irkutsk
8.63	45.80	235	2	0	Ispra
-16.50	28.30	2367	0	0	Izana
55.78	24.07	1059	0	0	Jabal_Hafeet

132.88	-12.67	30	2	1	Jabiru
-62.75	-8.63	100	3	1	Jamari
-61.93	-10.08	162	3	1	Jaru_Reserve
-61.80	-10.87	100	3	1	Ji_Parana
-61.97	-10.88	100	3	1	Ji_Parana_UNIR
28.03	-26.18	1736	3	0	Joberg
-84.47	31.23	50	3	0	JonesERC
-106.52	32.35	1288	3	1	Jornada
-76.78	38.77	10	3	1	Jug_Bay
-96.62	39.10	341	3	1	KONZA_EDC
73.47	4.97	0	3	2	Kaashidhoo
24.83	-14.87	1230	3	2	Kaloma
80.35	26.45	142	3	1	Kanpur
24.80	-14.78	1179	3	2	Kaoma
31.18	-10.17	1300	3	2	Kasama
-7.53	12.92	0	3	1	Katibougou
-65.28	44.38	154	2	0	Kejimkujik
-85.37	42.42	293	3	0	Kellogg_LTER
-80.17	25.73	0	3	0	Key_Biscayne
-74.48	39.80	50	3	0	Kolfield
23.78	35.53	0	0	0	Kolimbari
92.77	55.98	202	3	1	Krasnoyarsk
-77.80	55.30	0	3	2	Kuujjuarapik
-60.93	-14.57	170	3	1	LOS_FIEROS_98
-97.98	34.97	358	3	1	LW-SCAN
4.82	43.58	32	3	0	La_Crau
-117.25	32.87	115	3	0	La_Jolla
-67.03	17.97	0	3	1	La_Paguera
8.35	47.48	735	3	0	Laegeren
128.75	-16.12	150	3	1	Lake_Argyle
12.63	35.52	45	3	1	Lampedusa
-156.92	20.73	20	3	3	Lanai
18.10	40.33	0	3	0	Lecce_University
3.13	50.62	60	3	0	Lille
-122.60	49.03	0	3	0	Lochiel
15.65	78.22	30	3	2	Longyearbyen
-106.33	35.87	2350	3	1	Los_Alamos
-60.62	-14.55	225	2	2	Los_Fieros
-115.98	38.38	1908	3	0	Lunar_Lake
73.53	4.18	2	2	2	MALE
-76.62	39.28	15	3	1	MD_Science_Center
-118.25	34.25	450	3	0	MISR-JPL
-70.55	41.30	10	3	0	MVCO
-89.42	43.07	326	3	1	Madison
-111.97	33.07	360	3	1	Maricopa

5.38	43.28	100	3	0	Marseille
23.55	-19.90	940	0	0	Maun_Tower
-155.58	19.53	3397	0	0	Mauna_Loa
-99.18	19.33	2268	3	1	Mexico_City
53.78	23.15	204	3	1	Mezaira
31.93	-13.27	550	3	2	Mfuwe
-177.38	28.22	0	3	3	Midway_Island
27.50	53.00	200	3	1	Minsk
-114.08	46.92	1028	3	0	Missoula
10.93	44.63	56	3	0	Modena
28.82	47.00	205	3	1	Moldova
23.15	-15.25	1107	3	2	Mongu
-68.17	48.63	30	3	0	Mont_Joli
-121.87	36.58	50	3	0	Monterey
37.52	55.70	192	3	0	Moscow_MSU_MO
104.68	16.62	166	3	1	Mukdahan
11.27	48.22	520	3	0	Munich_Maisach
11.57	48.57	533	3	0	Munich_University
24.43	-11.73	1430	3	2	Mwinilunga
121.10	24.90	0	0	1	NCU_Taiwan
-98.28	55.90	290	3	1	NSA_YJP_BOREAS
166.92	-0.52	7	2	3	Nauru
28.67	-12.98	1270	3	2	Ndola
34.78	31.92	40	3	0	Nes_Ziona
-100.02	42.77	730	3	2	Niabrara
-76.27	36.85	20	3	0	Norfolk_State_Univ
137.13	37.33	200	3	0	Noto
-82.43	30.20	0	3	0	OceolaNF
-82.13	30.73	0	3	0	OkefenokeeNWR
127.77	26.37	46	1	1	Okinawa
98.43	17.80	1120	0	0	Omkoi
2.92	51.22	23	3	0	Oostende
135.58	34.65	50	3	0	Osaka
-1.40	12.20	290	3	2	Ouagadougou
-117.87	36.48	1167	1	0	Owens_Lake
-75.93	37.28	8	3	0	Oyster
-105.50	53.50	503	2	1	Paddockwood
2.22	48.70	156	3	0	Palaiseau
-4.52	41.98	750	3	0	Palencia
-79.85	9.17	0	3	0	Panama_BCI
2.33	48.87	60	2	0	Paris
-78.08	40.73	401	3	1	Penn_State_Univ
-75.00	40.03	20	3	0	Philadelphia
29.45	-23.88	1200	3	1	Pietersburg

102.57	15.18	220	3	1	Pimai
-3.22	36.93	1252	0	0	Pitres
-48.00	-11.00	210	3	2	Porto_Nacional
-63.95	-8.77	110	3	1	Porto_Velho
-62.87	-9.28	80	3	1	Potosi_Mine
-115.97	38.50	1435	3	0	Railroad_Valley
-4.15	50.37	0	3	1	Rame_Head
5.38	43.48	208	3	0	Realtor
-122.25	40.15	40	2	0	Red_Bluff
-116.98	46.48	824	3	0	Rimrock
-67.87	-9.97	212	3	2	Rio_Branco
-66.05	18.40	30	2	2	Rio_Piedras
-77.58	44.23	0	3	0	Rochester
-117.88	34.93	680	3	0	Rogers_Dry_Lake
12.65	41.83	130	3	0	Rome_Tor_Vergata
-65.60	18.20	10	3	1	Roosevelt_Roads
7.62	48.33	167	3	0	Rossfeld
115.30	-32.00	40	3	1	Rottnest_Island
-63.18	-17.80	442	3	0	SANTA_CRUZ
34.78	30.85	480	3	1	SEDE_BOKER
-76.50	38.88	10	3	1	SERC
31.58	-24.97	293	3	1	SKUKUZA_AEROPORT
-93.67	41.93	1030	3	1	SMEX
16.15	58.58	0	3	0	SMHI
-104.65	53.67	490	3	1	SSA_YJP_BOREAS
-119.48	33.27	133	3	0	San_Nicolas
-73.98	40.45	0	2	0	Sandy_Hook
-54.75	-2.43	70	2	1	Santarem
-70.72	-33.48	510	3	0	Santiago
-46.73	-23.57	865	2	0	Sao_Paulo
-123.13	48.78	200	3	0	Saturn_Island
23.28	-16.12	1025	3	2	Senanga
126.95	37.47	116	3	0	Seoul_SNU
24.30	-17.48	951	3	2	Sesheke
-106.88	34.35	1477	3	1	Sevilleta
-98.77	40.75	563	3	1	Shelton
135.37	33.68	10	3	1	Shirahama
-96.63	43.73	500	3	1	Sioux_Falls
54.23	25.22	10	3	1	Sir_Bu_Nuair
31.58	-24.98	150	3	1	Skukuza
46.42	24.92	650	3	1	Solar_Village
26.37	-12.17	1333	3	2	Solwezi
18.57	54.45	0	3	0	Sopot
-117.53	47.62	360	1	0	Spokane
-89.62	30.37	20	3	0	Stennis

-77.47	38.98	50	2	0	Sterling
26.07	-20.53	900	3	1	Sua_Pan
-55.20	5.80	0	2	1	Surinam
14.57	-22.67	250	2	0	Swakopmund
-117.68	34.38	2200	0	0	TABLE_MOUNTAIN_CA
8.68	35.55	1091	3	0	THALA
1.48	43.57	150	3	1	TOULOUSE
-105.23	40.12	1689	2	0	Table_Mountain
-149.62	-17.58	98	3	3	Tahiti
121.50	25.03	26	2	0	Taipei_CWB
0.08	43.25	350	3	0	Tarbes
-16.63	28.03	10	3	2	Tenerife
4.33	52.12	18	3	0	The_Hague
-97.85	55.80	218	3	2	Thompson
139.98	-28.98	38	3	1	Tinga_Tingana
-110.05	31.73	1408	3	1	Tombstone
85.05	56.48	130	3	2	Tomsk
26.47	58.27	70	3	1	Toravere
-79.47	43.97	300	3	0	Toronto
1.37	43.58	150	3	1	Toulouse
-110.95	32.23	779	3	0	Tucson
-49.68	-3.72	100	1	1	Tukurui
-118.45	34.07	131	3	0	UCLA
-119.85	34.42	33	3	0	UCSB
-76.88	39.03	50	3	1	USDA
-48.28	-18.90	850	3	1	Uberlandia
-118.92	45.13	1100	3	0	Ukiah
92.08	49.97	1363	3	2	Ulaangom
55.67	25.53	20	3	1	Umm_Al_Quwain
12.52	45.32	10	3	0	Venise
5.77	43.72	304	3	0	Vinon
-84.28	35.97	365	3	0	Walker_Branch
-75.47	37.93	10	3	0	Wallops
-106.08	53.92	550	3	2	Waskesiu
28.22	-26.33	1775	3	0	Wits_University
116.97	39.75	36	3	1	XiangHe
109.72	38.28	1080	3	1	Yulin
23.12	-13.53	1040	3	2	Zambezi